Hofstadter Topology with Real Space Invariants and Reentrant Projective Symmetries

Jonah Herzog-Arbeitman, Zhi-Da Song, Luis Elcoro, and B. Andrei Bernevig

Phys. Rev. Lett. **130**, 236601 — Published 6 June 2023

DOI: 10.1103/PhysRevLett.130.236601

Hofstadter Topology with Real Space Invariants and Reentrant Projective Symmetries

Jonah Herzog-Arbeitman[1], Zhi-Da Song[1,2], Luis Elcoro[3,4], and B. Andrei Bernevig[1,5,6]
[1]*Department of Physics, Princeton University, Princeton, NJ 08544*
[2]*International Center for Quantum Materials, School of Physics, Peking University, Beijing 100871, China*
[3]*Department of Physics, University of the Basque Country UPV/EHU, Apdo. 644, 48080 Bilbao, Spain*
[4]*EHU Quantum Center, University of the Basque Country UPV/EHU*
[5]*Donostia International Physics Center, P. Manuel de Lardizabal 4, 20018 Donostia-San Sebastian, Spain and*
[6]*IKERBASQUE, Basque Foundation for Science, Bilbao, Spain*
(Dated: May 12, 2023)

Adding magnetic flux to a band structure breaks Bloch's theorem by realizing a projective representation of the translation group. The resulting Hofstadter spectrum encodes the non-perturbative response of the bands to flux. Depending on their topology, adding flux can enforce a bulk gap closing (a Hofstadter semimetal) or boundary state pumping (a Hofstadter topological insulator). In this work, we present a real-space classification of these Hofstadter phases. We give topological indices in terms of symmetry-protected Real Space Invariants (RSIs), which reveal the bulk and boundary responses of fragile topological states to flux. In fact, we find that the flux periodicity in tight-binding models causes the symmetries which are broken by the magnetic field to reenter at strong flux where they form projective point group representations. We completely classify the reentrant projective point groups and find that the Schur multipliers which define them are Arahanov-Bohm phases calculated along the bonds of the crystal. We find that a nontrivial Schur multiplier is enough to predict and protect the Hofstadter response with only zero-flux topology.

Introduction. The magnetic translation group[1] is a famous example of how symmetries acquire projective representations in quantum mechanics, dramatically altering the behavior of the system. When magnetic flux is threaded through a two-dimensional crystal, the translation operators T_i along the ith lattice vector no longer commute and instead form a *projective* group

$$T_1T_2 = e^{i\phi}T_2T_1, \qquad \phi = \frac{e}{\hbar}\oint \mathbf{A}\cdot d\mathbf{r}, \tag{1}$$

where $\mathbf{A}$ is the vector potential of the magnetic field, e is the electron charge, and the flux ϕ is the Aharanov-Bohm phase difference between the two paths around the unit cell[2]. The square lattice[3] provides a concrete realization of Eq. (1), which results in a fractal energy spectrum known as the Hofstadter Butterfly. In this work, we find that point group (PG) symmetries can also be projective in strong flux. Their representations constrain the Hofstadter butterfly of a generic model in the paradigm of Hofstadter topology[4], where magnetic flux acts as a pumping parameter (a third dimension)[5–7]. We classify Hofstadter semimetals (SMs) with protected gap closings and Hofstadter higher order topological insulators (HOTIs) with boundary state pumping in all magnetic PGs. Their topological indices are written in terms of real space invariants (RSIs)[8–11] calculated with and without flux. Hofstadter physics has garnered attention from many directions[12–42], especially with the profusion of experiments on moiré materials[43–52] up to 2π flux[53]. Our results offer a unified, symmetry-based approach[54,55] to the problem while shedding new light on 2D topology.

Hamiltonians. The Hofstadter Hamiltonian H^ϕ describes electrons in a constant perpendicular magnetic field via the Peierls substitution[56,57]. We choose units where $\hbar, e$, and the unit cell area equal one, so $\phi = \nabla\times\mathbf{A}$. Consider a hopping term $\langle\mathbf{r}'|H|\mathbf{r}\rangle = t_{\mathbf{r}\mathbf{r}'}$, where $|\mathbf{r}\rangle$ an electron state at $\mathbf{r}$. Under the Peierls substitution, $\langle\mathbf{r}'|H^\phi|\mathbf{r}\rangle = t_{\mathbf{r}\mathbf{r}'}\exp i\int_{\mathbf{r}}^{\mathbf{r}'}\mathbf{A}\cdot d\mathbf{r}$. The "Peierls path" along which the integral is taken can be determined by the Wannier functions of the zero-field groundstate[58] and in the simplest case is a straight line. Because the Peierls paths are determined by the ground state electron density, the paths themselves respect the lattice symmetries. The spectrum of H^ϕ is gauge-invariant but depends on the Peierls paths. Importantly, $H^{\phi+\Phi} = UH^\phi U^\dagger$ has a nontrivial periodicity in flux[4], where

$$U|\mathbf{r}\rangle = \exp\left(i\int_{\mathbf{r}_0}^{\mathbf{r}}\mathbf{A}^\Phi\cdot d\mathbf{r}\right)|\mathbf{r}\rangle, \quad \nabla\times\mathbf{A}^\Phi = \Phi \tag{2}$$

where $\mathbf{r}_0$ is the position of an arbitrary but fixed orbital, and the integral is taken along (any) sequence of Peierls paths. Thus the spectrum is periodic in $\Phi\in 2\pi\mathbb{N}$, defined such that all closed integrals along Peierls paths enclose a multiple of 2π flux and U is single-valued (Fig. 1). For nearest neighbor hoppings on the square lattice, $\Phi = 2\pi$.

Symmetries. We now discuss the symmetries of crystalline systems composed of n-fold rotations C_n, mirrors $M = M_x, M_y$, and anti-unitary time reversal $\mathcal{T}$. In nonzero flux, the symmetries divide into two categories (see Fig. 2). M and $\mathcal{T}$ flip the sign of ϕ while rotations preserve it, so $C_n\mathcal{T}$ and M are broken but C_n and $M\mathcal{T}$ remain in flux (see[59] and references[60–67] therein). The symmetries broken in flux play a crucial role in the Hofstadter spectrum. In fact, these symmetries are *reentrant* at strong flux $\phi = \Phi/2$. If $[C_n\mathcal{T}, H^{\phi=0}] = 0$, then

$$UC_n\mathcal{T}H^{\Phi/2}(UC_n\mathcal{T})^{-1} = UH^{-\Phi/2}U^\dagger = H^{\Phi/2} \tag{3}$$

so $UC_n\mathcal{T}$ is a symmetry of $H^{\Phi/2}$. The same is true for UM and $U\mathcal{T}$. Since U is a diagonal unitary matrix in the

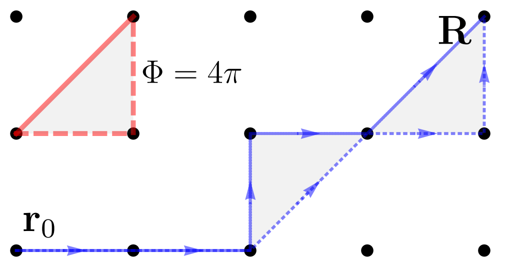

FIG. 1. Square lattice with nearest neighbor (dashed red) and diagonal (solid red) hoppings. With straight line Peierls paths, $\Phi = 2\pi \times 2$ because the minimal loop (shaded red) encloses area 1/2, shaded gray. In blue, we show examples of the flux-Φ string created by U from $\mathbf{r}_0$ to an orbital at $\mathbf{R}$. The path of the flux string is unobservable and may be deformed arbitrarily along Peierls paths because the difference in flux (shaded blue) is a multiple of 2π.

orbital basis and $\mathcal{T}$ acts locally on the orbitals, we have $(U\mathcal{T})^2 = \mathcal{T}^2$[4]. These reentrant symmetries can form a projective representation of the point group G_x.

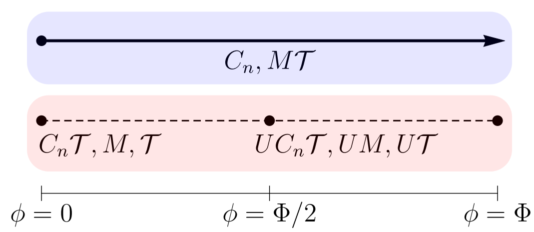

FIG. 2. PG symmetries preserved (blue) and broken (red) in flux. At multiples of $\Phi/2$, the broken symmetries are reentrant as implemented by the flux periodicity operator U.

Consider a Wyckoff position $\mathbf{x}$ and fix $\mathbf{A}(\mathbf{r}) = \frac{\phi}{2}\hat{z} \times (\mathbf{r} - \mathbf{x})$ to be in the symmetric gauge centered at $\mathbf{x}$ so the $C_n \in G_x$ operator remains unchanged in flux (see[59]). To determine the group structure of the symmetries at $\phi = \Phi/2$, we derive[59] the commutation relation

$$C_n^\dagger U C_n = e^{i\gamma_{\mathbf{x}}} U, \quad \gamma_{\mathbf{x}} = \frac{1}{n} \int_{\mathcal{C}_{\mathbf{x}}} \mathbf{A}^\Phi \cdot d\mathbf{r} \mod 2\pi \tag{4}$$

from Eq. (2) where $\mathcal{C}_{\mathbf{x}}$ is a C_n-symmetric loop *taken along Peierls paths* enclosing $\mathbf{x}$. We prove that $\gamma_{\mathbf{x}}$ is independent of the choice of loop[59], but we emphasize that $\gamma_{\mathbf{x}}$ depends on the Wyckoff position $\mathbf{x}$. Note that $\gamma_{\mathbf{x}} \in \frac{2\pi}{n}\mathbb{Z}_n$ is quantized because all closed loops along Peierls paths enclose multiples of 2π flux. If $|\lambda\rangle$ is an eigenstate of $H^{\phi=0}$ with C_n eigenvalue λ, then $U|\lambda\rangle$ is an eigenstate of H^Φ since $H^\Phi = UH^{\phi=0}U^\dagger$. The eigenvalue of $U|\lambda\rangle$ is

$$C_n U|\lambda\rangle = e^{-i\gamma_{\mathbf{x}}} U C_n |\lambda\rangle = \lambda e^{-i\gamma_{\mathbf{x}}} U|\lambda\rangle \tag{5}$$

so $\gamma_{\mathbf{x}} \neq 0$ indicates angular momentum is transferred with flux, indicating irrep flow. Finally, if there is an orbital of the Hamiltonian located at $\mathbf{x}$, then we can shrink the loop $\mathcal{C}_{\mathbf{x}}$ to be a single point, and hence $\gamma_{\mathbf{x}} = 0$ (see Fig. 3a). Conventional straight-line Peierls paths can have nontrivial $\gamma_{\mathbf{x}}$, as shown in Fig. 3b where $\gamma_{1a} = 0$ but $\gamma_{1b} = \pi$. When referring to a fixed PG and Wyckoff position, we will drop the $\mathbf{x}$ subscript.

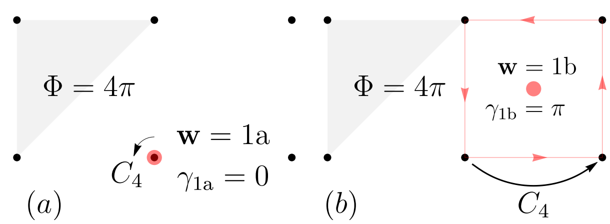

FIG. 3. Calculating $\gamma_{\mathbf{x}}$ at $\mathbf{x} = 1a, 1b$ on the square lattice with Peierls paths given in Fig. 1 which enforce $\Phi = 4\pi$. (a) At the 1a position (black), $\gamma_{1a} = 0$. (b) At the 1b position, $\gamma_{1b} = \pi$, which we calculate using Eq. (4) by choosing a C_4-symmetric path around the unit cell on nearest-neighbor Peierls paths. If we considered an alternate model without the diagonal Peierls path, then $\Phi = 2\pi$ and $\gamma_{1b} = \pi/2$.

The reentrant symmetries $UC_n\mathcal{T}$ and UM can form nontrivial central extensions of the conventional PGs at $\Phi/2$ flux when $\gamma \neq 0$, leading to projective representations which we call *non-crystalline*. In the context of group theory, γ is referred to as the Schur multiplier or 2-cocyle of the central extension. For instance, consider the PG $G_x = 41'$ which is generated by C_4 and $\mathcal{T}$. Let us now consider $\phi = \Phi/2$ where the point symmetries generating $G_x^{\Phi/2}$ are C_4 and $U\mathcal{T}$. These symmetries can generate a projective representation of $41'$ which we denote by $4_\gamma 1', \gamma = \pi/2, \pi, 3\pi/2$. We build their irreps from the C_4 eigenstates $|\lambda\rangle$ in Eq. (5). Using Eq. (4), $C_4 U\mathcal{T}|\lambda\rangle = e^{-i\gamma}\lambda^* U\mathcal{T}|\lambda\rangle$. If $\lambda \neq e^{-i\gamma}\lambda^*$, then $|\lambda\rangle$ and $U\mathcal{T}|\lambda\rangle$ must be distinct states which carry a 2D irrep since they are transformed to each other by C_4. If $\gamma = \pi/2$, there are two 2D irreps which we denote by ${}^1EA$ and ${}^2EB$ (see Table I). If $\gamma = \pi$, we find a 2D irrep AB and two 1D irreps ${}^1E, {}^2E$. From the group theory perspective, $4_\pi 1'$ is actually not a nontrivial central extension: it can be lifted to the non-projective group $41'$ by taking $C_4 \to iC_4$. However, this redefinition is not physically permissible: the overall phase of C_4 is fixed by the angular momenta (mod 4) of the orbitals in the basis, e.g. C_4 acts as $+1$ on s orbitals, for all values of the flux. Thus while $41'$ and $4_\pi 1'$ are isomorphic as groups, they are physically different. In $41'$, ${}^1E{}^2E$ corresponds to p_x-p_y orbitals, while in $4_\pi 1'$, AB corresponds to s-d orbitals, and the transition between the two groups enforces irrep flow. We enumerate all of the non-crystalline PGs and their irreps in Ref.[59], finding 51 non-crystalline PGs reentrant in magnetic flux, in comparison to the 31 crystalline PGs at zero flux. We note that the projective group $2_\pi mm$ first appeared in Ref.[68], where the nontrivial Schur multiplier was crucial for the calculation of the bulk quadrupole moment. All PGs and their irreps appear on the Bilbao Crystallographic Server[69].

Hofstadter Response of an Obstructed Atomic State. The symmetry and topology of $H^{\phi=0}$ determine the flux

$41'$	1	C_4	C_2
A	1	1	1
B	1	-1	1
${}^1E{}^2E$	2	0	-2

$4_{\pi/2}1'$	1	C_4	C_2
${}^1EA$	2	$1-i$	0
${}^2EB$	2	$-1+i$	0

$4_{\pi}1'$	1	C_4	C_2
AB	2	0	2
${}^1E$	1	$-i$	-1
${}^2E$	1	i	-1

TABLE I. We list the (partial) character tables for the irreps of $41'$ and two of its projective representations without SOC. (The irreps of $4_{3\pi/2}1'$ are the complex conjugates of $4_{\pi/2}1'$.) We name the irreps according to their C_4 eigenvalues where $A, B, {}^1E, {}^2E$ correspond to $+1, -1, -i, i$ respectively.

response and hence have a fundamental effect on the Hofstadter spectrum. A nonzero mirror Chern number enforces a bulk gap closing in finite flux[4,50,70–72] and a nonzero Kane-Mele index enforces edge state pumping in flux for $\Phi/2\pi$ odd, while a trivial atomic state remains gapped[4]. We now show that symmetry-protected analogues of these phases also exist. Their topological invariants may be found in[59].

We first study the Hofstadter SM state which is defined by an enforced gap closing at finite flux $\phi \in (0, \Phi)$. We consider a fixed Wyckoff position with PG G_x at zero flux, $G_x^{\Phi/2}$ at $\Phi/2$ flux, and $G_x^\phi \subseteq G_x$ at generic flux. In a Hofstadter SM, the bulk gap is closed in ϕ when a level crossing occurs. To avoid eigenvalue repulsion, the crossing states must be different irreps of G_x^ϕ, and thus the ground states before and after the crossing have different irreps. Before showing formally how RSIs detect this irrep exchange, we give a simple example.

Consider a Hamiltonian on open boundary conditions with s orbitals at corners of a square (four 1a sites). The center is the x =1b position and has $G_x = 41'$. We include nearest and second nearest neighbors with straight-line Peierls paths in flux, exactly as in Fig. 3b. In the symmetric gauge centered at 1b, we obtain (see[59])

$$H_4^\phi = \begin{pmatrix} 0 & te^{-i\phi/4} & t' & te^{i\phi/4} \\ te^{i\phi/4} & 0 & te^{-i\phi/4} & t' \\ t' & te^{i\phi/4} & 0 & te^{-i\phi/4} \\ te^{-i\phi/4} & t' & te^{i\phi/4} & 0 \end{pmatrix} . \tag{6}$$

The diagonal hopping t' sets $\Phi = 4\pi$ and $\gamma_{1b} = \pi$ (Fig. 3b). The symmetries at $\phi = 0$ are C_4 which permutes the sites around 1b and $\mathcal{T} = K$ which is complex conjugation. C_4 remains a symmetry for all ϕ, but $\mathcal{T}$ is broken in flux. Although the spectrum is 4π-periodic, the eigenstates are not. Eq. (5) shows there is irrep flow, e.g. if the lowest energy eigenstate of H_4 at $\phi = 0$ is an A irrep, then at $\phi = \Phi$ the lowest energy eigenstate is a B irrep because $\gamma_{1b} = \pi$. In this case, the ground state has changed irreps although C_4 symmetry is never broken, but this is only possible if there is a gap closing in flux. This gap closing can also be predicted entirely from the projective symmetries at $\phi = \Phi/2 = 2\pi$. There $U\mathcal{T}$ reenters as a symmetry with $U = \mathrm{diag}(1, -1, 1, -1)$ computed from Eq. (2). Table I shows that at $\phi = \Phi/2$, the PG is $4_\pi 1'$ which has the irrep AB, so the level crossing occurs at exactly $\phi = \Phi/2$ where the A and B irreps are degenerate (see Fig. 4). In this example, the Hofstadter SM phase was deduced from only zero-flux data: a nonzero Schur multiplier and the irreps of the ground state of $H^{\phi=0}$ enforced irrep flow at Φ and a gap closing exactly at $\Phi/2$. We call such phases "Peierls-indicated."

In this decoupled example, the multiplicities of each irrep at $x = 1b$ characterized the whole ground state. In a general Hamiltonian with nontrivial bands where the number of irreps at a Wyckoff position is not adiabatically well-defined, we use RSIs to study irrep flow. Defined in Ref.[8], RSIs are linear combinations of the momentum space irrep multiplicities at the high-symmetry points of the occupied bands, and thus are invariant under symmetry-preserving perturbations that do not close the gap. They contain local information about the Wannier state representations at each Wyckoff position. Indeed, the RSIs can be equivalently computed in real space on open boundary conditions[11] from the Wannier states at x and are invariant under G_x-allowed deformations that change the occupied irreps at x. For instance in $G_x = 41'$, four Wannier states in the representation $A \oplus B \oplus {}^1E{}^2E$ can be moved off x because they form an induced representation of the lower symmetry position[8]. However, the RSIs $\delta_i = \{m(B) - m(A), m({}^1E{}^2E) - m(A)\}$ are invariant under this process and are determined by the momentum space irreps. Here $m(\rho)$ is the multiplicity of the irrep ρ. In general, RSIs are invariant unless the gap is closed (changing the occupied states discontinuously) or the symmetries protecting them are broken. The RSIs of the non-crystalline PGs are computed in Ref.[59] using the Smith Normal form[8]. We now formalize the Hofstadter SM invariants using RSIs. To do so, we assume that the $\phi = 0$ ground state is gapped and has vanishing Chern number $C = 0$ so that integer-valued *local* RSIs are well-defined[8]. From the Streda formula[73,74] $C\phi/2\pi = n \mod 1$, $C = 0$ means we only consider fixed integer fillings for all ϕ. Here n is the fractional number of electrons per unit cell. If $n \notin \mathbb{N}$, then $C \neq 0$. Chern insulators were shown earlier to yield Hofstadter semimetals[4] whose gap closing occurs at $\phi \leq 2\pi/|C|$[50].

Hofstadter SM. Previously, we exemplified how C_n enforces a gap closing due to irrep flow (equivalently, a change of RSIs) in the occupied states. Generally, with M and $\mathcal{T}$ which relate the spectrum at $\pm\phi$, we obtain a finer classification by comparing the RSIs at $\phi = 0, \Phi/2$ denoted $\delta^{\phi=0}, \delta^{\phi=\Phi/2}$. A gap closing can be detected by an incompatibility of the RSIs $\delta^{\phi=0}$ and $\delta^{\phi=\Phi/2}$ when reduced to the G_x^ϕ subgroup. Perturbing away from $\phi = 0$ or $\phi = \Phi/2$, the PG is reduced to G_x^ϕ as the symmetries that reverse the flux are broken. The occupied states do not change under this infinitesimal perturbation (since $C = 0$), and the RSIs of G_x^ϕ can be determined from $\delta^{\phi=0}$ and $\delta^{\phi=\Phi/2}$ by irrep reduction[8]. We denote the RSIs determined from the reduction of $G_x \to G_x^\phi$ and $G_x^{\Phi/2} \to G_x^\phi$ as $\delta_i^{\phi\to 0}$ and $\delta_i^{\phi\to\Phi/2}$ respectively (i indexes the RSIs of G_x^ϕ). The Hofstadter SM index is

$$\delta_i^{SM} = \delta_i^{\phi\to 0} - \delta_i^{\phi\to\Phi/2} . \tag{7}$$

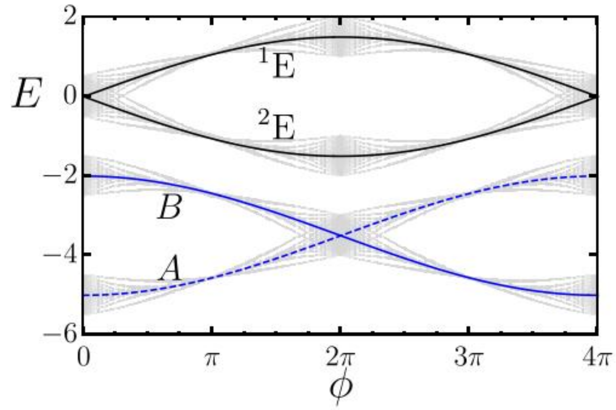

FIG. 4. Hofstadter spectrum of an obstructed atomic state whose Peierls paths give $\Phi = 4\pi, \gamma_{1b} = \pi$. The flat band limit is analytically solvable (see[59]) and is shown in blue (valence bands) and black (conduction bands). Small terms can be added to broaden the bands, and the Hofstadter spectrum in this case is shown in gray. In the flat band limit where the valence bands are compact Wannier functions, each is labeled by its C_4 irrep with a crossing at $\Phi/2$. Note that the ${}^1E{}^2E$ irrep protected by $\mathcal{T}$ is broken by flux.

We prove Eq. (7) from the properties of the RSIs. If there is no gap closing between 0 and $\Phi/2$ flux, then the RSIs of G_x^ϕ cannot change because the symmetries of G_x^ϕ exist at all flux. Hence if $\delta_i^{SM} \neq 0$, a gap closing must occur to change the occupied states. With C_n symmetry alone, the gap closings from irrep flow are detected formally by Hofstadter SM index $\delta_i^{\phi=0} - \delta_i^{\phi=\Phi}$, which can be written solely in terms of $\delta^{\phi=0}$ since the irreps at Φ are determined by U[59]. Moreover, we check exhaustively that Eq. (7) also diagnoses the gap closings protected by irrep flow (even though they only compare RSIs at 0 and $\Phi/2$ flux) due to the degeneracies protected at $\phi = \Phi/2$. We list the Hofstadter SM indices in all PGs in[59], finding $\mathbb{Z}$ indices with C_n and $\mathbb{Z}_2$ indices with $M\mathcal{T}$.

We illustrate Eq. (7) with H_4^ϕ. Table IIV in Ref.[59] contains the RSIs of $G_x = 41'$ and $G_x^{\Phi/2} = 4_\pi 1'$ (see[59] for examples of the calculation). Their reduction to the RSIs of $G_x^\phi = 4$ follows from ${}^1E{}^2E \to {}^1E \oplus {}^2E$ near $\phi = 0$ and $AB \to A \oplus B$ near $\phi = \Phi/2$ (see Table I). Using Eq. (7), we find a $\mathbb{Z}^3$ Hofstadter SM index:

$$\delta_i^{SM} = \{\delta_1^{\phi=0}, \delta_2^{\phi=0} + \delta_2^{\phi=\frac{\Phi}{2}}, \delta_2^{\phi=0} - \delta_1^{\phi=\frac{\Phi}{2}} + \delta_2^{\phi=\frac{\Phi}{2}}\} \ . \tag{8}$$

We see that the SM phase is Peierls-indicated because $\delta_1^{\phi=0} \neq 0$ enforces a gap closing, i.e. any zero-flux state with $\gamma_{1b} = \pi$ and $\delta_1^{\phi=0} = m(B) - m(A) \neq 0$ at the 1b Wyckoff position is a Hofstadter SM. This is exactly the same gap closing diagnosed by irrep flow, since A and B irreps exchange between $\phi = 0$ and $\phi = \Phi$. We generalize H_4 to a full lattice model in an obstructed atomic phase (see[59]) and show the protected crossings in Fig. 4.

Hofstadter HOTI. We now consider the Hofstadter HOTI phase defined by nontrivial flow of Wannier states

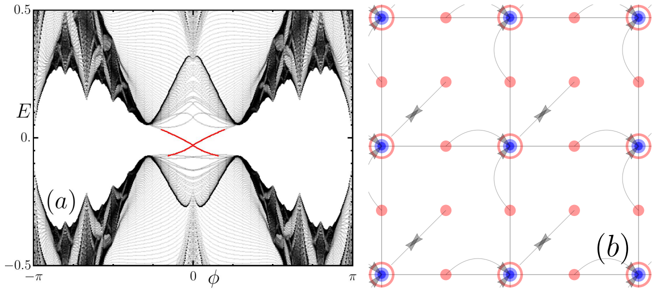

FIG. 5. Hofstadter HOTI with $C_2\mathcal{T}$. (a) Spectrum of a perturbed QSH model on 30×30 open boundary conditions with $\Phi = 2\pi, \gamma_{1d} = \pi$. The degenerate corner states at $\phi = 0$ are pumped into the bulk according to $\delta_{1d}^{HOTI} = 1 \bmod 2$. (b) Cartoon of bulk Wannier flow from $\phi = 0$ (red) to $\phi = \pi$ (blue). The dots represent electron Wannier centers, and the red hollow circle represents a hole Wannier center reflecting the fragile topology at $\phi = 0$. Flux breaks $C_2\mathcal{T}$, allowing the Wannier states to flow off the Wyckoff positions. The fragile topology at $\phi = 0$ is trivialized as the electron and hole Wannier states meet and annihilate, yielding a trivial atomic state at $\phi = \pi$ enforced by $(UC_2\mathcal{T})^2 = -1$ at the 1b position.

through the bulk over $\phi \in (0, \Phi/2)$. On open boundary conditions, this flow is manifested as a pumping cycle of edge/corner states into the bulk. For the Wannier states to evolve continuously, we require that $\delta_i^{SM} = 0$ at all Wyckoff positions so that there is no enforced bulk gap closing (see Eq. (7)). We develop topological invariants for these phases by detecting charge flow onto/off of a given Wyckoff position between $\phi = 0$ and $\Phi/2$. Explicitly, we compute the number of Wannier states at $\mathbf{x}$ by counting their representations:

$$N_{\mathbf{x}} = \sum_{\rho \in G_{\mathbf{x}}} m(\rho) \dim(\rho) \ . \tag{9}$$

Of course, $N_{\mathbf{x}}$ is not an adiabatic invariant because Wannier states can move onto and off of $\mathbf{x}$ if they form an induced representation. However $N_{\mathbf{x}}$ is adiabatically conserved modulo the dimension of the induced representation[8]. For instance, in PG $41'$, $N_{\mathbf{x}} \bmod 4$ is conserved (and can be written in terms of RSIs) because only multiples of 4 states can be moved while preserving C_4. Generally, we find that there exists $n_G \in \mathbb{N}$ such that

$$\delta_{\mathbf{x}}^{HOTI} = N_{\mathbf{x}}^{\phi=0} - N_{\mathbf{x}}^{\phi=\Phi/2} \mod n_G \tag{10}$$

can be written in terms of RSIs. Recall that a nonzero RSI off an orbital position diagnoses corner states on open boundary conditions[8,68,75,76]. Thus Eq. (10) diagnoses a Hofstadter HOTI phase because corner states are smoothly pumped onto/off of $\mathbf{x}$ if $\delta_{\mathbf{x}}^{HOTI} \neq 0$. In[59], we compute the compatibility conditions $\delta_i^{SM} = 0$ and then Hofstadter HOTI invariants for all PGs.

We now give an example in magnetic PG $2'$ without SOC and $\gamma_{\mathbf{x}} = \pi$, which can be obtained from the nearest-neighbor square lattice where $\Phi = 2\pi$, such as the quantum spin Hall (QSH) model[77]. PG $2'$ has a single irrep A where $D[C_2\mathcal{T}]=K$, which squares to $+1$. States can only be moved offsite in $C_2\mathcal{T}$-symmetric pairs, so the RSI protected by $C_2\mathcal{T}$ is $\delta = m(A) \mod 2$ and can be calculated from the nested Wilson loop[6,68,78] or the Stiefel-Whitney invariants[79–83]. At $\Phi/2$ flux, PG $2'_\pi$ has a single 2D irrep AA because $UC_2\mathcal{T}$ squares to -1. This PG has no RSI because the two states carrying AA can always be moved offsite in opposite directions while respecting $UC_2\mathcal{T}$. Correspondingly, the Wilson loop is always trivial[4]. In generic flux, $G^\phi = 1$ because $C_2\mathcal{T}$ is broken. Hence the gaps at $\phi=0$ and $\phi=\Phi/2$ are trivially compatible: $\delta_1^{SM}=0$. The total charge $N_{\mathbf{x}}$ is

$$N_{\mathbf{x}}^{\phi=0} = m(A) = \delta_1^{\phi=0} \bmod 2,\; N_{\mathbf{x}}^{\phi=\Phi/2} = 0 \bmod 2. \quad (11)$$

The Hofstadter HOTI invariant is simply $\delta_{\mathbf{x}}^{HOTI} = \delta_{\mathbf{x}}^{\phi=0} \in \mathbb{Z}_2$, and is Peierls-indicated. The HOTI index Eq. (11) describes a pumping process where a state pinned to $\mathbf{x}$ (which gives a corner state on open boundary conditions) is released as ϕ is increased and $C_2\mathcal{T}$ is broken. Fig. 5a shows an example of this phase using a perturbed QSH model (see[59]) with $C_2\mathcal{T}$-protected fragile topology showing corner modes (red) pumped into the bulk. Choosing straight-line paths on the square lattice, this model has $\Phi = 2\pi, \gamma_{1d} = \pi$ (in $p2'$, the 1d positon is $(1/2, 1/2)$) and hence has a Peierls-indicated Hofstadter HOTI phase. At $\phi=0$, mass terms added to the original QSH model break all symmetries except $C_2\mathcal{T}$ such that the two occupied bands have fragile topology indicated by nonzero RSIs $\delta_{\mathbf{x}}^{\phi=0} = 1 \mod 2$ at the four Wyckoff positions $\mathbf{x}$ =1a,1b,1c,1d[59]. Since $N_{\mathbf{x}}^{\phi=0} = \delta_{\mathbf{x}}^{\phi=0} \mod 2$, the nonzero RSIs identify a bound ±1 charge at each $\mathbf{x}$. Effectively, the RSIs protect a hole-like Wannier state with charge $-1 \bmod 2 = 1$ at one of the Wyckoff positions, yielding a total charge per unit cell of $1+1+1-1=2$ as required by the number of occupied bands. This is the fragile obstruction to an atomic limit, which is removed as flux breaks $C_2\mathcal{T}$, allowing the hole-like Wannier state to move off its Wyckoff position, annihilate, and reach the trivial state at $\phi=\pi$ enforced by $(UC_2\mathcal{T})^2=-1$.

Discussion. The appearance of projective symmetries in strong flux enables zero-flux RSIs to constrain the Hofstadter spectrum. This work has completely classified the resulting 51 non-crystalline 2D PGs and demonstrated that the symmetries and topology of $H^{\phi=0}$, encoded in the RSIs, dictate universal features of its spectrum in flux. Our results give observable bulk signatures of obstructed atomic and fragile phases. Although we have focused on crystalline systems, acoustic materials offer alternative platforms where projective symmetries have already gathered interest[84–88]. Indeed, the projective representation of $C_2\mathcal{T}$ has already been experimentally achieved[84,89] and synthetic gauge fields in these platforms have been used to experimentally confirm irrep flow due[90,91]. Additionally, we note that the Hofstadter topological indices derived here depend only on the local PG symmetries, and thus still apply to high-symmetry points in quasi-crystalline systems without translations[92–95]. Lastly, the ever expanding family of moiré materials has already allowed access to the strong flux regime where signatures of the reentrant symmetries have been proposed[96] and reentrant phases observed[53]. The single-particle projective symmetries unveiled here may also be approximately realized in continuum models[97,98], giving rise to otherwise impossible many-body phenomena in strong flux[58,99–101].

Note Added. A manuscript posted on the same day (Ref.[102]) also studies the topology of Hofstadter bands in magnetic flux. Ref.[102] employs a momentum space topological quantum chemistry approach at π flux and obtains stable invariants in certain wallpaper groups. Instead, we work in real space and classify Hofstadter responses in flux for all (projective) point group symmetries.

Acknowledgements. B.A.B. and Z-D.S. were supported by the European Research Council (ERC) under the European Union's Horizon 2020 research and innovation programme (grant agreement No. 101020833), the ONR Grant No. N00014-20-1-2303, the Schmidt Fund for Innovative Research, Simons Investigator Grant No. 404513, the Packard Foundation, the Gordon and Betty Moore Foundation through the EPiQS Initiative, Grant GBMF11070 and Grant No. GBMF8685 towards the Princeton theory program. Further support was provided by the NSF-MRSEC Grant No. DMR-2011750, BSF Israel US foundation Grant No. 2018226, and the Princeton Global Network Funds. JHA is supported by a Hertz Fellowship and thanks the Marshall Aid Commemoration Commission for support during the earlier stages of this project.

1. J. Zak. Magnetic translation group. *Phys. Rev.*, 134:A1602–A1606, Jun 1964. doi: 10.1103/PhysRev.134.A1602. URL `https://link.aps.org/doi/10.1103/PhysRev.134.A1602`.
2. Y. Aharonov and D. Bohm. Significance of electromagnetic potentials in the quantum theory. *Phys. Rev.*, 115: 485–491, Aug 1959. doi:10.1103/PhysRev.115.485. URL `https://link.aps.org/doi/10.1103/PhysRev.115.485`.
3. Douglas R. Hofstadter. Energy levels and wave functions of bloch electrons in rational and irrational magnetic fields. *Phys. Rev. B*, 14:2239–2249, Sep 1976. doi: 10.1103/PhysRevB.14.2239. URL `https://link.aps.org/doi/10.1103/PhysRevB.14.2239`.
4. Jonah Herzog-Arbeitman, Zhi-Da Song, Nicolas Regnault, and B. Andrei Bernevig. Hofstadter topology: Noncrystalline topological materials at high flux. *Phys. Rev. Lett.*, 125:236804, Dec 2020. doi: 10.1103/PhysRevLett.125.236804. URL `https://link.aps.org/doi/10.1103/PhysRevLett.125.236804`.
5. D. J. Thouless. Quantization of particle trans-

port. *Phys. Rev. B*, 27:6083–6087, May 1983. doi:10.1103/PhysRevB.27.6083. URL `https://link.aps.org/doi/10.1103/PhysRevB.27.6083`.

[6] Benjamin J. Wieder and B. Andrei Bernevig. The Axion Insulator as a Pump of Fragile Topology. *arXiv e-prints*, art. arXiv:1810.02373, Oct 2018.

[7] Julian F. Wienand, Friederike Horn, Monika Aidelsburger, Julian Bibo, and Fabian Grusdt. Thouless Pumps and Bulk-Boundary Correspondence in Higher-Order Symmetry-Protected Topological Phases. *Phys. Rev. Lett.*, 128(24):246602, June 2022. doi:10.1103/PhysRevLett.128.246602.

[8] Zhi-Da Song, Luis Elcoro, and B. Andrei Bernevig. Twisted bulk-boundary correspondence of fragile topology. *Science*, 367(6479):794–797, February 2020. doi:10.1126/science.aaz7650.

[9] Jonah Herzog-Arbeitman, Valerio Peri, Frank Schindler, Sebastian D. Huber, and B. Andrei Bernevig. Superfluid Weight Bounds from Symmetry and Quantum Geometry in Flat Bands. *Phys. Rev. Lett.*, 128(8):087002, February 2022. doi:10.1103/PhysRevLett.128.087002.

[10] Yuanfeng Xu, Luis Elcoro, Guowei Li, Zhi-Da Song, Nicolas Regnault, Qun Yang, Yan Sun, Stuart Parkin, Claudia Felser, and B. Andrei Bernevig. Three-Dimensional Real Space Invariants, Obstructed Atomic Insulators and A New Principle for Active Catalytic Sites. *arXiv e-prints*, art. arXiv:2111.02433, November 2021.

[11] Jonah Herzog-Arbeitman, B. Andrei Bernevig, and Zhi-Da Song. Interacting Topological Quantum Chemistry in 2D: Many-body Real Space Invariants. *arXiv e-prints*, art. arXiv:2212.00030, November 2022.

[12] Daniel Parker, Patrick Ledwith, Eslam Khalaf, Tomohiro Soejima, Johannes Hauschild, Yonglong Xie, Andrew Pierce, Michael P. Zaletel, Amir Yacoby, and Ashvin Vishwanath. Field-tuned and zero-field fractional Chern insulators in magic angle graphene. *arXiv e-prints*, art. arXiv:2112.13837, December 2021.

[13] Mark T. Mitchison, Ángel Rivas, and Miguel A. Martin-Delgado. Robust nonequilibrium surface currents in the 3D Hofstadter model. *arXiv e-prints*, art. arXiv:2201.11586, January 2022.

[14] Yoonseok Hwang, Jun-Won Rhim, and Bohm-Jung Yang. Geometric characterization of anomalous Landau levels of isolated flat bands. *Nature Communications*, 12:6433, November 2021. doi:10.1038/s41467-021-26765-z.

[15] Yuxuan Zhang, Naren Manjunath, Gautam Nambiar, and Maissam Barkeshli. Fractional disclination charge and discrete shift in the Hofstadter butterfly. *arXiv e-prints*, art. arXiv:2204.05320, April 2022.

[16] Jonathan Schirmer, C. X. Liu, and J. K. Jain. Phase diagram of superconductivity in the integer quantum Hall regime. *arXiv e-prints*, art. arXiv:2204.11737, April 2022.

[17] Daniel Shaffer, Jian Wang, and Luiz H. Santos. Unconventional Self-Similar Hofstadter Superconductivity from Repulsive Interactions. *arXiv e-prints*, art. arXiv:2204.13116, April 2022.

[18] Axel Fünfhaus, Thilo Kopp, and Elias Lettl. Winding vectors of topological defects: Multiband Chern numbers. *arXiv e-prints*, art. arXiv:2205.01406, May 2022.

[19] Manisha Arora, Rashi Sachdeva, and Sankalpa Ghosh. Hofstadter butterflies in magnetically modulated graphene bilayer: An algebraic approach. *Physica E Low-Dimensional Systems and Nanostructures*, 142:115311, August 2022. doi:10.1016/j.physe.2022.115311.

[20] Peizhi Mai, Edwin W. Huang, Jiachen Yu, Benjamin E. Feldman, and Philip W. Phillips. Interaction-driven Spontaneous Ferromagnetic Insulating States with Odd Chern Numbers. *arXiv e-prints*, art. arXiv:2205.08545, May 2022.

[21] Yifei Guan, Oleg V. Yazyev, and Alexander Kruchkov. Re-entrant magic-angle phenomena in twisted bilayer graphene in integer magnetic fluxes. *arXiv e-prints*, art. arXiv:2201.13062, January 2022.

[22] Luke Yeo and Philip J. D. Crowley. Non-power-law universal scaling in incommensurate systems. *arXiv e-prints*, art. arXiv:2206.02810, June 2022.

[23] R. Mosseri, R. Vogeler, and J. Vidal. Aharonov-Bohm cages, flat bands, and gap labelling in hyperbolic tilings. *arXiv e-prints*, art. arXiv:2206.04543, June 2022.

[24] Rasoul Ghadimi, Takanori Sugimoto, and Takami Tohyama. Higher-dimensional Hofstadter butterfly on Penrose lattice. *arXiv e-prints*, art. arXiv:2207.03028, July 2022.

[25] Jie Wang, Jiawei Zang, Jennifer Cano, and Andrew J. Millis. Staggered Pseudo Magnetic Field in Twisted Transition Metal Dichalcogenides: Physical Origin and Experimental Consequences. *arXiv e-prints*, art. arXiv:2110.14570, October 2021.

[26] Yifei Guan, Adrien Bouhon, and Oleg V. Yazyev. Landau Levels of the Euler Class Topology. *arXiv e-prints*, art. arXiv:2108.10353, August 2021.

[27] Tomonari Mizoguchi, Yoshihito Kuno, and Yasuhiro Hatsugai. Flat band, spin-1 Dirac cone, and Hofstadter diagram in the fermionic square kagome model. *Phys. Rev. B*, 104(3):035161, July 2021. doi:10.1103/PhysRevB.104.035161.

[28] Yoshiyuki Matsuki, Kazuki Ikeda, and Mikito Koshino. Fractal defect states in the Hofstadter butterfly. *Phys. Rev. B*, 104(3):035305, July 2021. doi:10.1103/PhysRevB.104.035305.

[29] QuanSheng Wu, Jianpeng Liu, Yifei Guan, and Oleg V. Yazyev. Landau levels as a probe for band topology in graphene moiré superlattices. *Phys. Rev. Lett.*, 126:056401, Feb 2021. doi:10.1103/PhysRevLett.126.056401. URL `https://link.aps.org/doi/10.1103/PhysRevLett.126.056401`.

[30] Kuan-Sen Lin and Barry Bradlyn. Simulating higher-order topological insulators in density wave insulators. *Phys. Rev. B*, 103(24):245107, June 2021. doi:10.1103/PhysRevB.103.245107.

[31] Zheng-Wei Zuo, Wladimir A. Benalcazar, Yunzhe Liu, and Chao-Xing Liu. Topological phases of the dimerized Hofstadter butterfly. *Journal of Physics D Applied Physics*, 54(41):414004, October 2021. doi:10.1088/1361-6463/ac12f7.

[32] Qiao-Ru Xu, Emilio Cobanera, and Gerardo Ortiz. Bloch and Bethe ansatze for the Harper model: A butterfly with a boundary. *arXiv e-prints*, art. arXiv:2107.10393, July 2021.

[33] Yuria Otaki and Takahiro Fukui. Higher-order topological insulators in a magnetic field. *Phys. Rev. B*, 100(24):245108, December 2019. doi:10.1103/PhysRevB.100.245108.

[34] Faruk Abdulla, Ankur Das, Sumathi Rao, and Ganpathy Murthy. Time-reversal-broken Weyl semimetal in the Hofstadter regime. *arXiv e-prints*, art. arXiv:2108.03196, August 2021.

[35] Biao Lian, Fang Xie, and B. Andrei Bernevig.

Open momentum space method for the Hofstadter butterfly and the quantized Lorentz susceptibility. *Phys. Rev. B*, 103(16):L161405, April 2021. doi: 10.1103/PhysRevB.103.L161405.

[36] Daniel Shaffer, Jian Wang, and Luiz H. Santos. Theory of Hofstadter superconductors. *Phys. Rev. B*, 104(18):184501, November 2021. doi: 10.1103/PhysRevB.104.184501.

[37] Koichi Asaga and Takahiro Fukui. Boundary-obstructed topological phases of a massive Dirac fermion in a magnetic field. *Phys. Rev. B*, 102(15):155102, October 2020. doi:10.1103/PhysRevB.102.155102.

[38] Irakli Titvinidze, Julian Legendre, Maarten Grothus, Bernhard Irsigler, Karyn Le Hur, and Walter Hofstetter. Spin-orbit coupling in the kagome lattice with flux and time-reversal symmetry. *Phys. Rev. B*, 103(19):195105, May 2021. doi:10.1103/PhysRevB.103.195105.

[39] Sheng Li, Xiao-Xue Yan, Jin-Hua Gao, and Yong Hu. Circuit QED simulator of two-dimensional Su-Schrieffer-Hegger model: magnetic field induced topological phase transition in high-order topological insulators. *arXiv e-prints*, art. arXiv:2109.12919, September 2021.

[40] Y. Otaki and T. Fukui. Higher order topological insulators in a magnetic field. *arXiv e-prints*, art. arXiv:1908.10976, Aug 2019.

[41] Simon Becker, Lingrui Ge, and Jens Wittsten. Hofstadter butterflies and metal/insulator transitions for moiré heterostructures. *arXiv e-prints*, art. arXiv:2206.11891, June 2022.

[42] Elliott H. Lieb. Flux phase of the half-filled band. *Phys. Rev. Lett.*, 73(16):2158–2161, October 1994. doi: 10.1103/PhysRevLett.73.2158.

[43] Jiachen Yu, Benjamin A. Foutty, Zhaoyu Han, Mark E. Barber, Yoni Schattner, Kenji Watanabe, Takashi Taniguchi, Philip Phillips, Zhi-Xun Shen, Steven A. Kivelson, and Benjamin E. Feldman. Correlated hofstadter spectrum and flavor phase diagram in magic angle graphene, 2021.

[44] Robin Huber, Max-Niklas Steffen, Martin Drienovsky, Andreas Sandner, Kenji Watanabe, Takashi Taniguchi, Daniela Pfannkuche, Dieter Weiss, and Jonathan Eroms. Brown-zak and weiss oscillations in a gate-tunable graphene superlattice: A unified picture of miniband conductivity, 2021.

[45] Joe Finney, Aaron L. Sharpe, Eli J. Fox, Connie L. Hsueh, Daniel E. Parker, Matthew Yankowitz, Shaowen Chen, Kenji Watanabe, Takashi Taniguchi, Cory R. Dean, Ashvin Vishwanath, Marc Kastner, and David Goldhaber-Gordon. Unusual magnetotransport in twisted bilayer graphene, 2021.

[46] Hryhoriy Polshyn, Yuxuan Zhang, Manish A. Kumar, Tomohiro Soejima, Patrick Ledwith, Kenji Watanabe, Takashi Taniguchi, Ashvin Vishwanath, Michael P. Zaletel, and Andrea F. Young. Topological charge density waves at half-integer filling of a moiré superlattice, 2021.

[47] Cheng Shen, Jianghua Ying, Le Liu, Jianpeng Liu, Na Li, Shuopei Wang, Jian Tang, Yanchong Zhao, Yanbang Chu, Kenji Watanabe, and et al. Emergence of chern insulating states in non-magic angle twisted bilayer graphene. *Chinese Physics Letters*, 38(4):047301, May 2021. ISSN 1741-3540. doi:10.1088/0256-307x/38/4/047301. URL `http://dx.doi.org/10.1088/0256-307X/38/4/047301`.

[48] Jeong Min Park, Yuan Cao, Kenji Watanabe, Takashi Taniguchi, and Pablo Jarillo-Herrero. Flavour hund's coupling, chern gaps and charge diffusivity in moiré graphene. *Nature*, 592(7852):43–48, Mar 2021. ISSN 1476-4687. doi: 10.1038/s41586-021-03366-w. URL `http://dx.doi.org/10.1038/s41586-021-03366-w`.

[49] Xiaobo Lu, Jian Tang, John R. Wallbank, Shuopei Wang, Cheng Shen, Shuang Wu, Peng Chen, Wei Yang, Jing Zhang, Kenji Watanabe, and et al. High-order minibands and interband landau level reconstruction in graphene moiré superlattices. *Physical Review B*, 102(4), Jul 2020. ISSN 2469-9969. doi:10.1103/physrevb.102.045409. URL `http://dx.doi.org/10.1103/PhysRevB.102.045409`.

[50] G. William Burg, Biao Lian, Takashi Taniguchi, Kenji Watanabe, B. Andrei Bernevig, and Emanuel Tutuc. Evidence of Emergent Symmetry and Valley Chern Number in Twisted Double-Bilayer Graphene. *arXiv e-prints*, art. arXiv:2006.14000, June 2020.

[51] Xiaobo Lu, Biao Lian, Gaurav Chaudhary, Benjamin A. Piot, Giulio Romagnoli, Kenji Watanabe, Takashi Taniguchi, Martino Poggio, Allan H. MacDonald, B. Andrei Bernevig, and Dmitri K. Efetov. Multiple Flat Bands and Topological Hofstadter Butterfly in Twisted Bilayer Graphene Close to the Second Magic Angle. *arXiv e-prints*, art. arXiv:2006.13963, June 2020.

[52] Ipsita Das, Xiaobo Lu, Jonah Herzog-Arbeitman, Zhi-Da Song, Kenji Watanabe, Takashi Taniguchi, B. Andrei Bernevig, and Dmitri K. Efetov. Symmetry broken Chern insulators and magic series of Rashba-like Landau level crossings in magic angle bilayer graphene. *arXiv e-prints*, art. arXiv:2007.13390, July 2020.

[53] Ipsita Das, Cheng Shen, Alexandre Jaoui, Jonah Herzog-Arbeitman, Aaron Chew, Chang-Woo Cho, Kenji Watanabe, Takashi Taniguchi, Benjamin A. Piot, B. Andrei Bernevig, and Dmitri K. Efetov. Observation of reentrant correlated insulators and interaction-driven fermi-surface reconstructions at one magnetic flux quantum per moiré unit cell in magic-angle twisted bilayer graphene. *Phys. Rev. Lett.*, 128:217701, May 2022. doi: 10.1103/PhysRevLett.128.217701. URL `https://link.aps.org/doi/10.1103/PhysRevLett.128.217701`.

[54] Barry Bradlyn, L. Elcoro, Jennifer Cano, M. G. Vergniory, Zhijun Wang, C. Felser, M. I. Aroyo, and B. Andrei Bernevig. Topological quantum chemistry. *Nature (London)*, 547(7663):298–305, Jul 2017. doi: 10.1038/nature23268.

[55] Luis Elcoro, Benjamin J. Wieder, Zhida Song, Yuanfeng Xu, Barry Bradlyn, and B. Andrei Bernevig. Magnetic Topological Quantum Chemistry. *arXiv e-prints*, art. arXiv:2010.00598, October 2020.

[56] R. Peierls. Zur Theorie des Diamagnetismus von Leitungselektronen. *Zeitschrift fur Physik*, 80:763–791, November 1933. doi:10.1007/BF01342591.

[57] J. M. Luttinger. The effect of a magnetic field on electrons in a periodic potential. *Phys. Rev.*, 84:814–817, Nov 1951. doi:10.1103/PhysRev.84.814. URL `https://link.aps.org/doi/10.1103/PhysRev.84.814`.

[58] Biao Lian, Fang Xie, and B. Andrei Bernevig. The Landau Level of Fragile Topology. *arXiv e-prints*, art. arXiv:1811.11786, Nov 2018.

[59] See supplementary material for additional details, examples.

[60] Rafi Bistritzer and Allan H. MacDonald. Moiré bands in twisted double-layer graphene. *Proceedings of the National Academy of Science*, 108(30):12233–12237, Jul 2011. doi:10.1073/pnas.1108174108.

[61] Mikito Koshino, Noah F. Q. Yuan, Takashi Koretsune, Masayuki Ochi, Kazuhiko Kuroki, and Liang Fu. Maximally Localized Wannier Orbitals and the Extended Hubbard Model for Twisted Bilayer Graphene. *Physical Review X*, 8(3):031087, July 2018. doi: 10.1103/PhysRevX.8.031087.

[62] Jian Kang and Oskar Vafek. Symmetry, Maximally Localized Wannier States, and a Low-Energy Model for Twisted Bilayer Graphene Narrow Bands. *Physical Review X*, 8(3):031088, July 2018. doi: 10.1103/PhysRevX.8.031088.

[63] Mois I. Aroyo, Asen Kirov, Cesar Capillas, J. M. Perez-Mato, and Hans Wondratschek. Bilbao Crystallographic Server. II. Representations of crystallographic point groups and space groups. *Acta Crystallographica Section A*, 62(2):115–128, Mar 2006. doi: 10.1107/S0108767305040286. URL `https://doi.org/10.1107/S0108767305040286`.

[64] Luis Elcoro, Barry Bradlyn, Zhijun Wang, Maia G. Vergniory, Jennifer Cano, Claudia Felser, B. Andrei Bernevig, Danel Orobengoa, Gemma de la Flor, and Mois I. Aroyo. Double crystallographic groups and their representations on the Bilbao Crystallographic Server. *Journal of Applied Crystallography*, 50(5):1457–1477, Oct 2017. doi:10.1107/S1600576717011712. URL `https://doi.org/10.1107/S1600576717011712`.

[65] C.J. Bradley and A.P. Cracknell. *The Mathematical Theory of Symmetry in Solids: Representation Theory for Point Groups and Space Groups*. Clarendon Press, 1972. URL `https://books.google.com/books?id=OKXvAAAAMAAJ`.

[66] E. P. Wigner. Über die operation der zeitumkehr in der quantenmechanik. *Nachr. Akad. Wiss. Göttingen Math.-Phys. Kl.*, pages 546–559, 1932. doi:10.1007/978-3-662-02781-3˙15. URL `https://doi.org/10.1007/978-3-662-02781-3_15`.

[67] E.P. Wigner and J.J. Griffin. *Group Theory and Its Application to the Quantum Mechanics of Atomic Spectra*. Academic Press, 1959. URL `https://books.google.com/books?id=BZsEAQAAIAAJ`.

[68] Wladimir A. Benalcazar, B. Andrei Bernevig, and Taylor L. Hughes. Electric multipole moments, topological multipole moment pumping, and chiral hinge states in crystalline insulators. *Phys. Rev. B*, 96(24):245115, Dec 2017. doi:10.1103/PhysRevB.96.245115.

[69] Mois Ilia Aroyo, Juan Manuel Perez-Mato, Cesar Capillas, Eli Kroumova, Svetoslav Ivantchev, Gotzon Madariaga, Asen Kirov, and Hans Wondratschek. Bilbao crystallographic server: I. databases and crystallographic computing programs. *Zeitschrift für Kristallographie-Crystalline Materials*, 221(1):15–27, 2006.

[70] Song-Bo Zhang, Hai-Zhou Lu, and Shun-Qing Shen. Edge states and integer quantum Hall effect in topological insulator thin films. *Scientific Reports*, 5:13277, August 2015. doi:10.1038/srep13277.

[71] Song-Bo Zhang, Yan-Yang Zhang, and Shun-Qing Shen. Robustness of quantum spin Hall effect in an external magnetic field. *Phys. Rev. B*, 90(11):115305, September 2014. doi:10.1103/PhysRevB.90.115305.

[72] B. Andrei Bernevig and Taylor L. Hughes. *Topological Insulators and Topological Superconductors*. Princeton University Press, student edition edition, 2013. ISBN 9780691151755. URL `http://www.jstor.org/stable/j.ctt19cc2gc`.

[73] P Streda. Theory of quantised hall conductivity in two dimensions. *Journal of Physics C: Solid State Physics*, 15(22):L717–L721, aug 1982. doi: 10.1088/0022-3719/15/22/005. URL `https://doi.org/10.1088/0022-3719/15/22/005`.

[74] I Dana, Y Avron, and J Zak. Quantised hall conductance in a perfect crystal. *Journal of Physics C: Solid State Physics*, 18(22):L679–L683, aug 1985. doi: 10.1088/0022-3719/18/22/004. URL `https://doi.org/10.1088%2F0022-3719%2F18%2F22%2F004`.

[75] Matthew Proctor, Paloma Arroyo Huidobro, Barry Bradlyn, María Blanco de Paz, Maia G. Vergniory, Dario Bercioux, and Aitzol García-Etxarri. Robustness of topological corner modes in photonic crystals. *Physical Review Research*, 2(4):042038, December 2020. doi: 10.1103/PhysRevResearch.2.042038.

[76] Wladimir A. Benalcazar, Tianhe Li, and Taylor L. Hughes. Quantization of fractional corner charge in C_n-symmetric higher-order topological crystalline insulators. *Phys. Rev. B*, 99(24):245151, June 2019. doi: 10.1103/PhysRevB.99.245151.

[77] B. Andrei Bernevig, Taylor L. Hughes, and Shou-Cheng Zhang. Quantum Spin Hall Effect and Topological Phase Transition in HgTe Quantum Wells. *Science*, 314(5806): 1757, Dec 2006. doi:10.1126/science.1133734.

[78] Wladimir A. Benalcazar, B. Andrei Bernevig, and Taylor L. Hughes. Quantized electric multipole insulators. *Science*, 357(6346):61–66, Jul 2017. doi: 10.1126/science.aah6442.

[79] Junyeong Ahn, Sungjoon Park, Dongwook Kim, Youngkuk Kim, and Bohm-Jung Yang. Stiefel-Whitney classes and topological phases in band theory. *Chinese Physics B*, 28(11):117101, November 2019. doi: 10.1088/1674-1056/ab4d3b.

[80] Junyeong Ahn and Bohm-Jung Yang. Symmetry representation approach to topological invariants in $C_{2z}T$ -symmetric systems. *Phys. Rev. B*, 99(23):235125, June 2019. doi:10.1103/PhysRevB.99.235125.

[81] J. Ahn, S. Park, and B.-J. Yang. Failure of Nielsen-Ninomiya Theorem and Fragile Topology in Two-Dimensional Systems with Space-Time Inversion Symmetry: Application to Twisted Bilayer Graphene at Magic Angle. *Physical Review X*, 9(2):021013, April 2019. doi: 10.1103/PhysRevX.9.021013.

[82] Zhida Song, Zhijun Wang, Wujun Shi, Gang Li, Chen Fang, and B. Andrei Bernevig. All magic angles in twisted bilayer graphene are topological. *Phys. Rev. Lett.*, 123:036401, Jul 2019. doi: 10.1103/PhysRevLett.123.036401. URL `https://link.aps.org/doi/10.1103/PhysRevLett.123.036401`.

[83] Adrien Bouhon, Annica M. Black-Schaffer, and Robert-Jan Slager. Wilson loop approach to metastable topology of split elementary band representations and topological crystalline insulators with time reversal symmetry. *arXiv e-prints*, art. arXiv:1804.09719, Apr 2018.

[84] Yan Meng, Shuxin Lin, Bin-jie Shi, Bin Wei, Linyun Yang, Bei Yan, Zhenxiao Zhu, Xiang Xi, Yin Wang, Yong Ge, Shou-qi Yuan, Jingming Chen, Guigeng Liu, Hongxiang Sun, Hongsheng Chen, Yihao Yang, and Zhen Gao. Spinful topological phases in acoustic crystals with projective PT symmetry. *arXiv e-prints*, art. arXiv:2207.13000, July 2022.

[85] Haoran Xue, Zihao Wang, Yue-Xin Huang, Zheyu Cheng, Letian Yu, Y. X. Foo, Y. X. Zhao,

Shengyuan A. Yang, and Baile Zhang. Projectively enriched symmetry and topology in acoustic crystals. *Phys. Rev. Lett.*, 128:116802, Mar 2022. doi: 10.1103/PhysRevLett.128.116802. URL `https://link.aps.org/doi/10.1103/PhysRevLett.128.116802`.

[86] Tianzi Li, Juan Du, Qicheng Zhang, Yitong Li, Xiying Fan, Fan Zhang, and Chunyin Qiu. Acoustic Möbius insulators from projective symmetry. *arXiv e-prints*, art. arXiv:2107.14579, July 2021.

[87] Haoran Xue, Ding Jia, Yong Ge, Yi-jun Guan, Qiang Wang, Shou-qi Yuan, Hong-xiang Sun, Y. D. Chong, and Baile Zhang. Observation of dislocation-induced topological modes in a three-dimensional acoustic topological insulator. *arXiv e-prints*, art. arXiv:2104.13161, April 2021.

[88] L. B. Shao, Q. Liu, R. Xiao, Shengyuan A. Yang, and Y. X. Zhao. Gauge-field extended $k \cdot p$ method and novel topological phases. *Phys. Rev. Lett.*, 127:076401, Aug 2021. doi:10.1103/PhysRevLett.127.076401. URL `https://link.aps.org/doi/10.1103/PhysRevLett.127.076401`.

[89] Xiao Xiang, Feng Gao, Yugui Peng, Qili Sun, Jie Zhu, and Xuefeng Zhu. Acoustic mirror Chern insulator with projective parity-time symmetry. *arXiv e-prints*, art. arXiv:2209.02349, September 2022.

[90] Valerio Peri, Zhi-Da Song, Marc Serra-Garcia, Pascal Engeler, Raquel Queiroz, Xueqin Huang, Weiyin Deng, Zhengyou Liu, B. Andrei Bernevig, and Sebastian D. Huber. Experimental characterization of fragile topology in an acoustic metamaterial. *Science*, 367(6479):797–800, February 2020. doi:10.1126/science.aaz7654.

[91] Zhi-Kang Lin, Ying Wu, Bin Jiang, Yang Liu, Shiqiao Wu, Feng Li, and Jian-Hua Jiang. Experimental realization of single-plaquette gauge flux insertion and topological Wannier cycles. *arXiv e-prints*, art. arXiv:2105.02070, May 2021.

[92] Callum W. Duncan, Sourav Manna, and Anne E. B. Nielsen. Topological models in rotationally symmetric quasicrystals. *Phys. Rev. B*, 101:115413, Mar 2020. doi:10.1103/PhysRevB.101.115413. URL `https://link.aps.org/doi/10.1103/PhysRevB.101.115413`.

[93] Dean Johnstone, Matthew J. Colbrook, Anne E. B. Nielsen, Patrik Öhberg, and Callum W. Duncan. Bulk Localised Transport States in Infinite and Finite Quasicrystals via Magnetic Aperiodicity. *arXiv e-prints*, art. arXiv:2107.05635, July 2021.

[94] Hyunsoo Ha and Bohm-Jung Yang. Macroscopically degenerate localized zero-energy states of quasicrystalline bilayer systems in strong coupling limit. *arXiv e-prints*, art. arXiv:2103.08851, March 2021.

[95] Duc-Thanh Tran, Alexandre Dauphin, Nathan Goldman, and Pierre Gaspard. Topological Hofstadter insulators in a two-dimensional quasicrystal. *Phys. Rev. B*, 91(8):085125, February 2015. doi: 10.1103/PhysRevB.91.085125.

[96] Sun-Woo Kim, Sunam Jeon, Moon Jip Park, and Youngkuk Kim. Replica Higher-Order Topology of Hofstadter Butterflies in Twisted Bilayer Graphene. *arXiv e-prints*, art. arXiv:2204.08087, April 2022.

[97] Michael G. Scheer, Kaiyuan Gu, and Biao Lian. Magic angles in twisted bilayer graphene near commensuration: Towards a hypermagic regime. *Phys. Rev. B*, 106:115418, Sep 2022. doi:10.1103/PhysRevB.106.115418. URL `https://link.aps.org/doi/10.1103/PhysRevB.106.115418`.

[98] Huan Wang, Yadong Jiang, Zhaochen Liu, and Jing Wang. Moiré Engineering and Topological Flat Bands in Twisted Orbital-Active Bilayers. *arXiv e-prints*, art. arXiv:2209.06524, September 2022.

[99] Jonah Herzog-Arbeitman, Aaron Chew, Dmitri K. Efetov, and B. Andrei Bernevig. Reentrant Correlated Insulators in Twisted Bilayer Graphene at 25T (2π Flux). *arXiv e-prints*, art. arXiv:2111.11434, November 2021.

[100] Jonah Herzog-Arbeitman, Aaron Chew, and B. Andrei Bernevig. Magnetic Bloch Theorem and Reentrant Flat Bands in Twisted Bilayer Graphene at 2π Flux. *arXiv e-prints*, art. arXiv:2206.07717, June 2022.

[101] Daniel Shaffer, Jian Wang, and Luiz H. Santos. Theory of Hofstadter Superconductors. *arXiv e-prints*, art. arXiv:2108.04831, August 2021.

[102] Yuan Fang and Jennifer Cano. Symmetry indicators in commensurate magnetic flux. *arXiv e-prints*, art. arXiv:2209.10557, September 2022.